# Insights into $\pi$-Conjugated Small Molecule Neat Films and Blends As Determined Through Photoconductivity

**Jacek J. Jasieniak,[†,§] Ben B.Y. Hsu,[†] Christopher J. Takacs,[†] Gregory C. Welch,[‡] Guillermo C. Bazan,[‡] Daniel Moses,[†] and Alan J. Heeger[†,*]**

[†]Center for Polymers and Organic Solids and [‡]Department of Chemistry, University of California, Santa Barbara, California 93106, United States

**ABSTRACT**

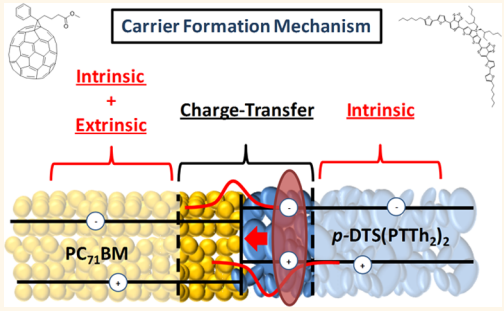


**Spectrally dependent steady-state photoconductivity is a convenient method to gain insight into the charge generation and transport processes within a given material. In this work, we report on the photoconductive response of solution-processed neat films and blends of the fullerene, $PC_{71}BM$, and the donor—acceptor small-molecule, $p$-DTS$(PTTh_2)_2$, as function of the processing additive, diiodooctane (DIO). The results, when considered in the context of their structural, optical, and electronic properties give insight into the dominant carrier generation and charge transport mechanisms in each of these molecular systems.**

**KEYWORDS:** small molecule · fullerene · photoconductivity · bulk heterojunction · binding energy · additive

Efficient bulk heterojunction (BHJ) solar cells comprise an interpenetrating network of donor and acceptor phases that can effectively charge separate photoexcited carriers and transport them to the cell electrodes.[1,2] The conventional approaches used to control the morphology of such blends, as to ensure the most efficient devices, have relied on the use of appropriate solvents,[3] temperature,[4] or solvent annealing[5] steps. We have shown that an alternative route, which enables finer-tuning of the evolving heterojunction dimensions, is through the use of molecular additives such as diiodooctane (DIO), octanedithiol, and chloronapthalene.[6,7] These additives are believed to modify the solubility of the components within the solution and during the deposition steps, thus enabling modification of the morphology.[7−10] In our more recent work, we have focused on the understanding of additive effects on small-molecule/fullerene based blends. One of the most successful blends of this type features 5,5′-*bis*{(4-(7-hexylthiophen-2-yl)thiophen-2-yl)-[1,2,5]thiadiazolo[3,4-c]-pyridine}-3,3′-di-2-ethylhexylsilylene-2,2′-bithiophene, $p$-DTS$(PTTh_2)_2$:[6,6]-phenyl $C_{71}$ butyric acid methyl ester, $PC_{71}BM$. Sun and co-workers demonstrated that through the use of only 0.25% v/v of DIO during the film forming process, solar cells with an optimum efficiency approaching 7% could be fabricated.[11] The small quantity of DIO was in this case found to result in a reduction of the $p$-DTS$(PTTh_2)_2$ nanocrystal size, which in turn enabled more efficient charge separation within the blend.

In BHJ compositions, the charge separation event has been conventionally assumed to occur *via* photoexcitation of Frenkel excitons which subsequently diffuse to a donor—acceptor interface.[12] This mechanism is not consistent with the femtosecond charge separation lifetimes that are observed in high efficiency BHJs.[13] Localized excitation of excitons which then diffuse, would require unrealistic diffusion constants (>2.5 $cm^2/s$) to achieve the observed charge separation lifetimes.[14] On the basis of ultrafast transient photoconductivity experiments, we have for many years concluded that extended states must form following the photoexcitation event in various $\pi$-conjugated systems.[15−18] Spectroscopic evidence from a number of groups have implied similar conclusions,[19−21]

[§] Permanent Address: CSIRO Materials Science and Engineering, Clayton, Victoria, 3168, Australia.

* Address correspondence to ajhe@physics.ucsb.edu.

Received for review May 31, 2012 and accepted September 13, 2012.

**Published online September 13, 2012**
**10.1021/nn303724m**

indicating that delocalization during the photoexcitation process enables long-range charge separation to occur in various bulk heterojunction systems.

Recent photoinduced absorption measurements have demonstrated ultrafast charge transfer at times less than 50 fs and, in addition, a slowly rising component which peaks at 100−500 ps then continues out to approximately 1 ns.[22] The ultrafast charge transfer originates from delocalized electrons and holes immediately following photon absorption, and the slower process is attributed to exciton hopping to a charge separating interface. Delocalization in $\pi$-conjugated systems, which must be determined by the extent of conjugation and the intermolecular packing, occurs on the nanometer scale.[23,24] Naturally, this entails that morphologies of this length scale are required for efficient charge separation.

Neat $\pi$-conjugated systems also exhibit charge separation, albeit to a lower extent than in efficient BHJs. The origin of this charge separation has been a contentious issue for decades. Part of the complexity in its understanding originates from the difficulty in decoupling extrinsic and intrinsic dissociation mechanisms.[25,26] In systems which possess very weak and disordered intermolecular interactions in the solid state, for example, regiorandom poly(3-hexylthiopehene), the primary photoexcitation must be localized within segments of a given conjugated polymer chain.[27]

In systems with reduced disorder and strong intermolecular interactions, for example, regioregular poly(3-hexylthiophene), *rr*-P3HT, primary electron and hole excitations occur with significant extended state character. This picture of the electronic structure is consistent with the lack of stimulated emission, negligible intersystem crossing, and low fluorescence yields that are observed in such systems.[27] In support of this excitation mechanism, temperature-dependent picosecond transient photoconductivity measurements have shown that free carrier formation occurs at experimentally limited time scales of less than 100 ps, and that these exhibit relatively high mobilities (30−40 $cm^2/(V\ s)$), at early time scales.[28]

A unified theoretical approach that can describe the primary photoexcitation mechanism in various molecular and polymeric systems as a function of their packing motifs, the intermolecular coupling and the level of disorder, is still lacking. Despite this, molecular engineering has continued to rapidly advance, driven largely through empirical classification based on solar cell performance and field-effect charge mobilities. As a result of the many trialed molecular platforms, donor−acceptor architectures have emerged as the archetypal feature in most molecular and polymeric systems that deliver high efficiency solar cells and exhibit high mobility transistors.[29] *p*-DTS$(PTTh_2)_2$ is one example of such a molecular system.

We have focused on understanding the photoinduced charge generation properties of this material in the presence of $PC_{71}BM$ using photovoltaic measurements.[11,30] Transient absorption measurements of the molecular derivative *d*-DTS$(PTTh_2)_2$ have shown that a 0.25% DIO (v/v) quantity results in the most rapid dissociation event;[31] a finding that is consistent with the most efficient *p*-DTS$(PTTh_2)_2$ based photovoltaic devices.[11] This indicates that the time scale of the photodissocation event is directly correlated to the morphology. Photovoltaic measurements directly probe the efficiency of the photoexcited charge-separation event and the collections of these carriers driven toward the electrodes by the built-in field within the vertical diode configuration.[32] For understanding the spectral photoresponse and ultimately the primary photoexciation mechanism of a given material, such device geometries may present problems due to contact effects and parasitic absorption contributions.[33] An arguably simpler measurement that obviates these issues is lateral photoconductivity.

The photoconductivity ($\sigma_{ph}$, S $cm^{-1}$) of any photoconductor is defined by eq 1, where *e* is the elementary charge (C), *n* is the steady-state density of photogenerated electrons (e) and holes (h) ($cm^{-3}$), and $\mu$ is their carrier mobility ($cm^2/(V\ s)$).

$$\sigma_{ph} = e(n_e\mu_e + n_h\mu_h) = (I_{ph}/A) \times (I/V) \quad (1)$$

Experimentally, $\sigma_{ph}$ is determined from the measured photocurrent ($I_{ph}$) of a photoconductor of cross-sectional area (*A*) and length (*l*), measured at an applied voltage (*V*). $\sigma_{ph}$ is directly proportional to the $n\mu$ product, with both *n* and $\mu$ being intrinsically related to the spectrally dependent optical and electronic properties of a given material.

In this work, we investigate the influence of the additive DIO on the photoconductive response of a *p*-DTS$(PTTh_2)_2$:$PC_{71}BM$ thin film cast from a solution mixture with a ratio of donor to acceptor of 7:3. This blend ratio results in the highest solar cell performance at an optimum DIO quantity of 0.25% v/v. As it is unclear whether the origin of this morphological "sweet-spot" is driven by a single component or through the interplay of both components, we also study the affect of this additive on neat $PC_{71}BM$ and *p*-DTS$(PTTh_2)_2$. By comparing these results with their structural, electrical transport, and absorption properties, we are able to get a more complete understanding of the role that DIO has on the photoconductivity in these systems, as well as gain insight into the mechanism of their primary photoexcitation event.

## RESULTS AND DISCUSSION

The experimental setup, the molecular structures of the molecules investigated, and the various thin-film compositions studied as a function of DIO concentration are included in Figure 1. For each of these molecular

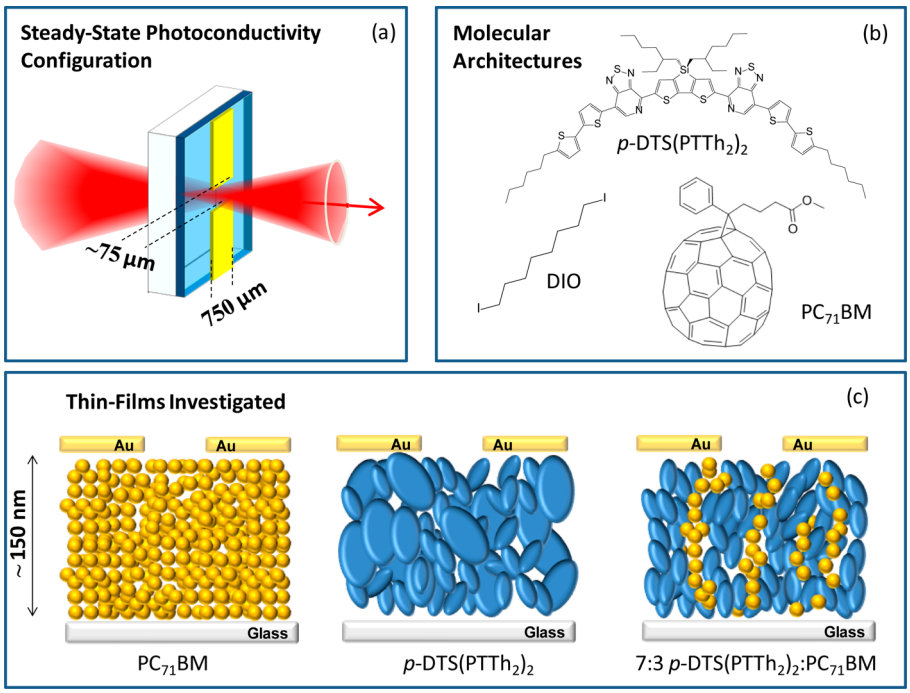


**Figure 1. (a) A schematic of the configuration used to measure steady-state photoconductivity of thin-films featuring the molecular architectures shown in panel b. (c) A depiction of the three material configurations, each with varying DIO concentration, investigated in this work *via* photoconductivity.**

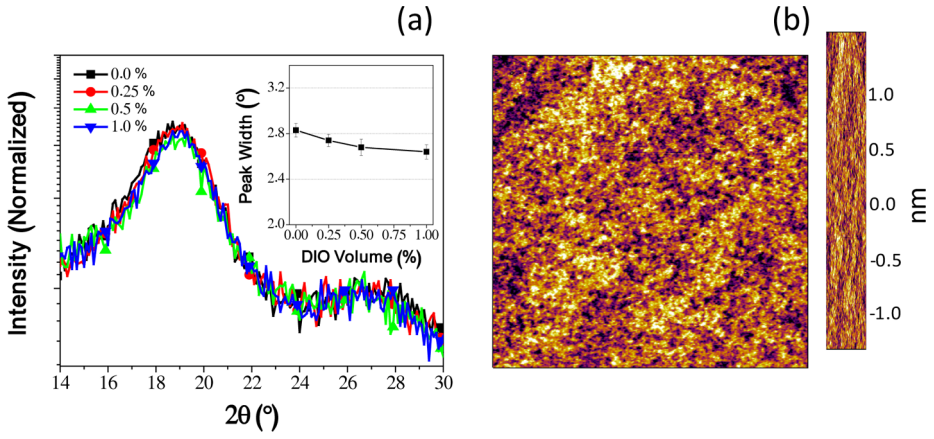


**Figure 2. (a) Out-of-plane X-ray diffraction of $PC_{71}BM$ thin-films as a function of DIO concentration in the deposition solution. (Inset) Gaussian peak width of the $2\theta \approx 18.9°$ ($d \approx 0.47$ nm) scattering contribution depicting changes to the long-range out-of-plane ordering in the sample. (b) A 4 $\mu m^2$ AFM micrograph of the 0% DIO $PC_{71}BM$ sample. The corresponding rms roughness of the sample is 0.51 nm.**

systems, we have gained insight into their structural properties through out-of-plane X-ray diffraction (XRD) measurements. In these measurements, we have utilized the peak width, determined through a Gaussian fit of the respective scattering peaks, as a relative measure of the order within our samples.

For completeness, we have also carried out atomic force microscopy (AFM) or high resolution transmission electron microscopy (HR-TEM) to gauge the surface topography or crystallinity within the samples, respectively. This structural understanding provides a more fundamental basis from which to appreciate the lateral photoconductivities measured for each of the materials. By further comparing these external photoconductive responses to the absorption within the thin films, we have determined their internal photoconductive properties. This latter quantity is defined as the quantum yield of collected photocarriers (*i.e.*, the number of collected electrons divided by the number of photons absorbed).

The magnitude and profile of the internal photoconductivity provide the necessary insight to probe the excitation and dissociation mechanisms within these systems. Because one of the goals of this research is to understand the influence of DIO on both of these mechanisms, we will now sequentially describe

the finding from each of the above measurements for $PC_{71}BM$, *p*-DTS$(PTTh_2)_2$, and *p*-DTS$(PTTh_2)_2$:$PC_{71}BM$ as a function of DIO, then provide a comparison to clarify the origin of photoconductivity in these systems.

**Influence of DIO on $PC_{71}BM$ Thin-Films.** In Figure 2a we present the XRD data of $PC_{71}BM$ thin-films as a function of DIO. Functionalized fullerene films have been shown to exhibit amorphous or nanocrystalline character at temperatures below 205 °C.[34] The scattering contributions at $2\theta \approx 18.9°$ ($d \approx 0.47$ nm), which is characteristic of such an amorphous or nanocrystalline matrix, exhibit only minor differences upon the utilization of the additive. This indicates that the inclusion of up to 1% DIO does not appear to significantly vary the structural properties of the neat $PC_{71}BM$ films.

The X-ray data are consistent with topographic studies using AFM. An exemplary micrograph of the 0% DIO samples is shown in Figure 2b to demonstrate this consistency. Across the entire additive range studied here, we found the surfaces to exhibit similar nanostructured topographies and root-mean-square (rms) roughness values of ~0.5 nm across a 4 $\mu m^2$ area.

This lack of large scale structural variation is reflected in the photoconductive responses which are shown in Figure 3a. To understand the internal photoconductive response, in Figure 3b we compare the photoconductive spectral profile of the 0.25% DIO sample with its thin-film absorptance spectrum (corresponding transmittance and reflectance spectra are included in the Supporting Information, Figure S1a). For clarity, we do not show the results of samples with other DIO concentrations because these were similar in both magnitude and profile. Instead, in Figure 3c we compare the calculated quantum efficiency for collected photocarriers for all the samples studied. The latter will be used as a means to quantitatively compare all the systems studied in this work.

For all the samples studied, good spectral agreement is observed close to the absorption edge (~1.75 eV) with a pronounced increase in the photoconductive response at higher energies (>2.2 eV). To ensure that the high energy enhancement in photoconductivity was not a result of direct photoemission, we performed photoconductive measurements in the presence of a $CO_2 + SF_6$ (9:1) quenching gas mixture (Supporting Information, Figure S2).[35] We did not observe any differences to the photoconductive response upon the introduction of this gas mixture. This confirms that the enhancement at energies larger than ~2.2 eV is due to an intrinsic phenomenon, such as, intermolecular or interband excitation.[36]

Recent studies using ultraviolet and inverse photoemission spectroscopies have shown that the electronic bandgap in $PC_{71}BM$ is 2.2 eV.[37] The remarkable agreement between the photoconductivity and the photoemission measurements corroborates our

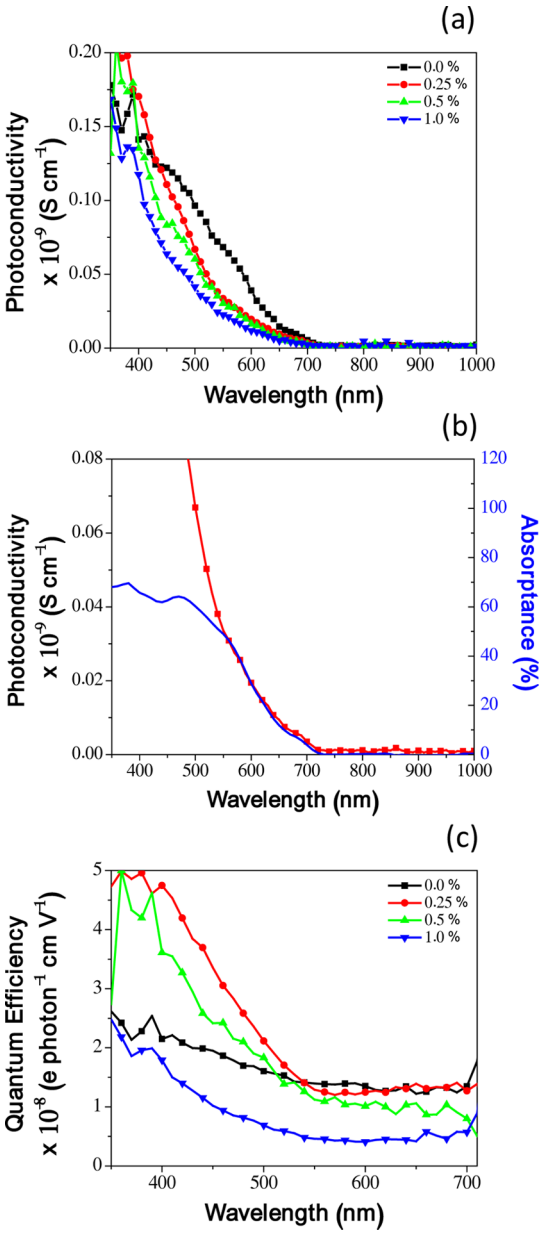


**Figure 3. (a) Steady-state photoconductive profiles of $PC_{71}BM$ as a function of DIO concentration. The photocurrents were renormalized to a constant incident photon flux of $10^{14}$ photons/cm$^2$ s (b) A comparison of the photoconductive response (red squares) of $PC_{71}BM$ with 0.25% DIO and its absorptance spectrum (—). (c) Calculated electric field dependent quantum yields for photocarrier collection, defined as a number of electrons collected per photon per electric field strength (V/cm), for $PC_{71}BM$ as a function of DIO concentration used during film forming. These yields were validated for electric fields up to 5 × $10^4$ V/cm.**

conclusions. On the basis of this value of the electronic bandgap, one determines the exciton binding energy in $PC_{71}BM$ to be ~0.45 eV—a value that is comparable to that in $C_{60}$.[36] This suggests that at energies close to the absorption onset, photoconductivity is most likely extrinsic in these systems.

**Influence of DIO on *p*-DTS$(PTTh_2)_2$ Thin-Films.** We now turn our attention to the influence of processing with DIO

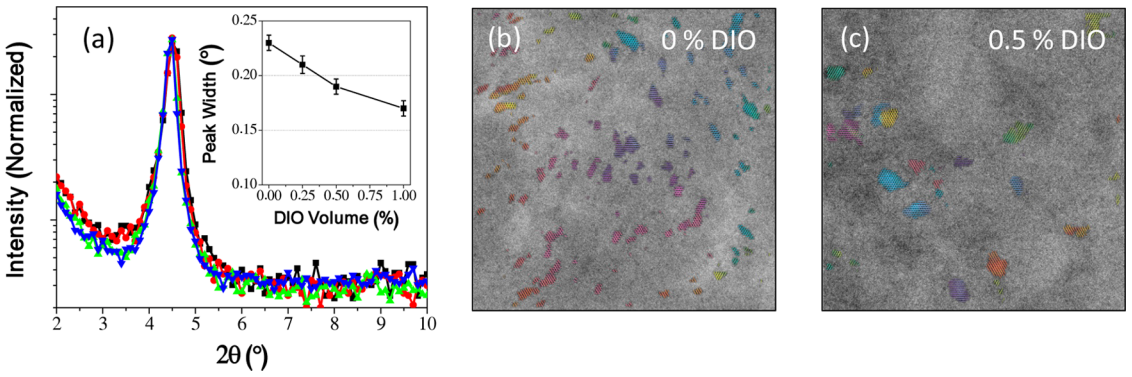


**Figure 4. (a) Out-of-plane X-ray diffraction of *p*-DTS(PTTh$_2$)$_2$ thin-films as a function of DIO concentration in the deposition solution. (Inset) Gaussian peak width of the $2\theta \approx 4.51°$ ($d \approx 1.96$ nm) scattering contribution. HR-TEM of the corresponding in-plane contributions for (b) 0% and (c) 0.5% DIO additive concentrations used during the deposition of *p*-DTS(PTTh$_2$)$_2$ thin-films. Colored lines have been added for clarity to denote the strength and directionality of the crystalline planes. Evidence for longer range correlation (>200 nm) is seen for the 0% DIO sample despite the reduced coherence length compared to the 0.5% DIO sample. The side length of each TEM image is 656 nm.**

on the structural and photoconductive properties of *p*-DTS(PTTh$_2$)$_2$ neat films. As shown in Figure 4a, the strong scattering contribution from the out-of-plane alkyl stacking at $2\theta \approx 4.51°$ ($d \approx 1.96$ nm) exhibits a gradual decrease in the peak width with increasing DIO concentration. This indicates that the use of DIO additive acts to gradually enhance the ordering of the out-of-plane alkyl stacking contribution within these thin-films. Using Scherrer analysis, these peak width values provide an estimation of the crystallite size which increases from ~35 to ~50 nm upon changing the DIO from 0% to 1% v/v.

HR-TEM was used to spatially resolve the in-plane orientation of the alkyl stacking population in *p*-DTS(PTTh$_2$)$_2$ thin-films. Images of samples prepared with 0% and 0.5% DIO additive are shown in Figure 4 panels b and c, respectively. Colored lines denoting the direction of the observed lattice planes have been overlaid for visual clarity. Striking, long-range correlations of neighboring crystallites are observed in the samples prepared with 0% v/v DIO over lengths scales much greater than 200 nm.

Increasing the [DIO] to 0.5% v/v both increases the size of the observed crystallites and reduces their apparent long-range correlations. We note that the degree of order is underestimated for the 0.5% sample due to beam induced drift of this sample. Similar indications of in-plane, long-range order for the $\pi-\pi$ "crystallite" populations are inferred using selected-area electron diffraction (see Supporting Information, Figure S3). These results are consistent with the X-ray diffraction data and indicate a high degree of nanostructure in both thin-films.

In Figure 5a we show how these structural changes translate to modifying the photoconductive properties of the *p*-DTS(PTTh$_2$)$_2$. Analogous to PC$_{71}$BM, the magnitude of the photoresponse was found to remain similar regardless of the additive concentration. Subtle variations to the spectral profile were, however, observed with samples processed with higher concentrations of DIO, specifically a slightly pronounced photoconductive peak at ~715 nm and a slightly narrower spectral response. Both of these features are consistent with the increased order in the *p*-DTS(PTTh$_2$)$_2$ with increasing DIO concentration.

To better appreciate this photoconductivity dependence on the morphology, we carried out field effect mobility measurements of *p*-DTS(PTTh$_2$)$_2$ as a function of [DIO] (Supporting Infromation, Table S1). The hole mobilities were found to remain nearly constant (within a factor of 3 across the entire [DIO] range), despite the variation in "crystallite" size. This observation is consistent with the fact that mobility is correlated with both long- and short-range structural correlation.[38,39] The HR-TEM suggests that the enhancement of the short-range correlation at high [DIO] arises at the cost of the long-range correlation. Ultimately, this structural modification minimizes the variation to the carrier mobilities within *p*-DTS(PTTh$_2$)$_2$. According to eq 1, this finding also indicates that the evolution of the morphology does not influence the steady-state density of photogenerated carriers.

A comparison of the photoconductive response to the absorptance of *p*-DTS(PTTh$_2$)$_2$ films processed with 0.25% (v/v) DIO is shown in Figure 5b (corresponding transmittance and reflectance spectra are included in the Supporting Information, Figure S1b). We find an almost quantitative agreement between the photoconductive response and the absorptance profile across the entire 1.8 eV window studied. The minor spectral variations observed within the first absorption manifold are likely associated with anisotropy within the films. Figure 5c shows the calculated electric field dependent quantum yields for photocarrier collection for *p*-DTS(PTTh$_2$)$_2$ as a function of [DIO]. These data clearly show that, in this system, both the magnitudes of the quantum efficiencies and their spectral profiles are independent of the morphology obtained within the additive range studied here.

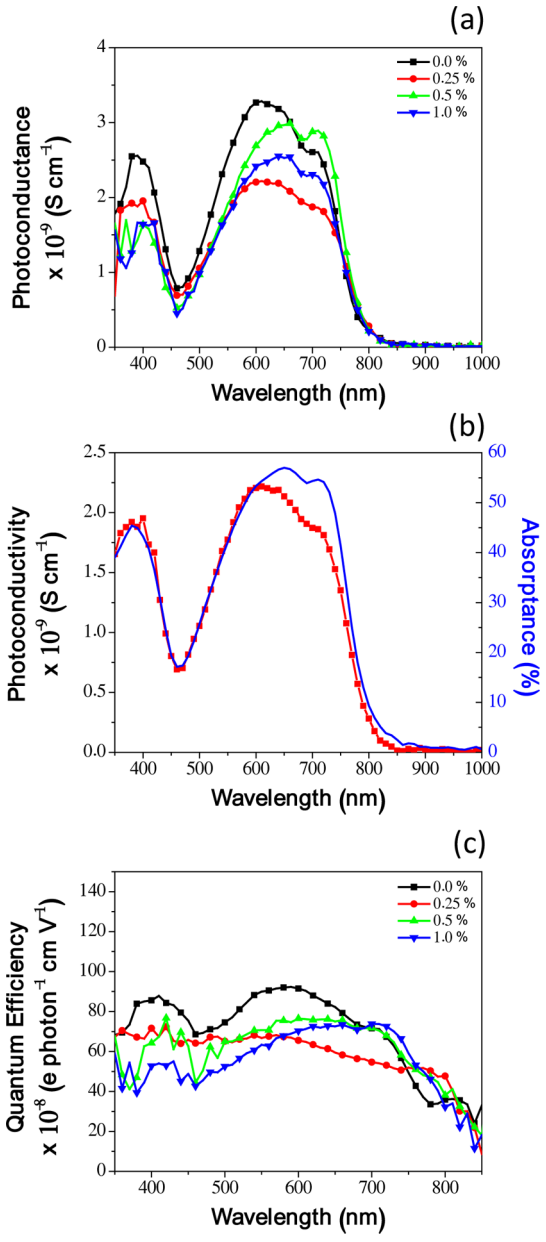


**Figure 5. (a) Steady-state photoconductive profiles of *p*-DTS($PTTh_2$)$_2$ as a function of DIO concentration. The photocurrents were renormalized to a constant incident photon flux of $10^{14}$ photons/cm$^2$ s (b) A comparison of the photoconductive response (red squares) of *p*-DTS($PTTh_2$)$_2$ with 0.25% DIO and corresponding absorptance spectrum (—). (c) Calculated electric field dependent quantum yields for photocarrier collection for *p*-DTS($PTTh_2$)$_2$ as a function of DIO concentration in the system. These yields were validated for electric fields up to $2 \times 10^4$ V/cm.**

**Influence of DIO on *p*-DTS($PTTh_2$)$_2$:$PC_{71}BM$ Thin-Films.** In Figure 6 we show the effect of DIO concentration on the long-range order of the 7:3 *p*-DTS($PTTh_2$)$_2$:$PC_{71}BM$ blend. Unlike for neat *p*-DTS($PTTh_2$)$_2$, in this system we observe distinctly different trends between the low (<0.5%) and high (≥0.5%) DIO regimes. X-ray scattering (Figure 6a) shows that at low DIO quantities the alkyl stacking peak width is minimally impacted, while in the high [DIO] regime a pronounced decrease in its value is found. The enhanced coherence length between these two [DIO] regions is highlighted in Figure 6b,c through HR-TEM of blends prepared using solutions containing 0% and 0.6% DIO v/v. Consistent with the X-ray data, the micrographs exhibit a clear increase in the "crystallite" size at the higher [DIO].

At intermediate [DIO], the "crystallite" sizes are highly sensitive to the additive concentration, and have in fact been found to reduce slightly in size at the nominal value of 0.25% DIO.[11] This sensitivity of the crystallite size indicates that the interplay between the $PC_{71}BM$, *p*-DTS($PTTh_2$)$_2$ and DIO governs the morphological evolution in a vastly different way than the pure small-molecule films with DIO. At 0% v/v DIO, this factor is exemplified by the fact that nucleated crystallites do not possess any obvious long-range ordering in blends compared to the neat films.[40] Furthermore, blends fabricated with 1% DIO v/v exhibit a significantly narrower out-of-plane alkyl stacking scattering peak (longer coherence length) than neat *p*-DTS($PTTh_2$)$_2$. These combined factors hint that the complex morphological evolutions of the blends are influenced by heterogeneous nucleation events.

Photoconductivity measurements of these DTS($PTTh_2$)$_2$:$PC_{71}BM$ BHJ systems as a function of DIO concentration are shown in Figure 7a. In contrast to the individual constituents, but consistent with the morphological evolution, the BHJ samples exhibited a strong dependence on DIO concentration. This dependence is exemplified with a nearly 4 fold increase in the photoconductive response with only 0.25% DIO, followed by a 10-fold drop with an increase up to 1%. While the levels of sensitization vary slightly, these results are generally consistent with those observed in photovoltaic measurements.[11] This highlights that despite the conductive pathways being lateral in our photoconductivity measurements, the outcome of the morphological evolution is similarly reflected through both lateral and vertical conduction.

Finally, in Figure 7b we compare the spectral response of the 0.25% DIO BHJ thin-film to its absorptance (corresponding transmittance and reflectance spectra are included in the Supporting Information, Figure S1c). While the magnitude of the photoconductivity within the blend is enhanced by orders of magnitude over that of the pure material (see following section), a clear suppression of the *p*-DTS($PTTh_2$)$_2$ photoconductive response within the blend is observed. This is associated with an enhanced quantum efficiency of collected charges within the 400−500 nm spectral region (Figure 7c). As this region is dominated by the $PC_{71}BM$ contribution, we can state that it is contributing more strongly to the photocurrent in the lateral direction than *p*-DTS($PTTh_2$)$_2$. This is not the case in photovoltaic measurements, where charge separation and collection is observed to be more strongly representative of both components.[11] On the basis of

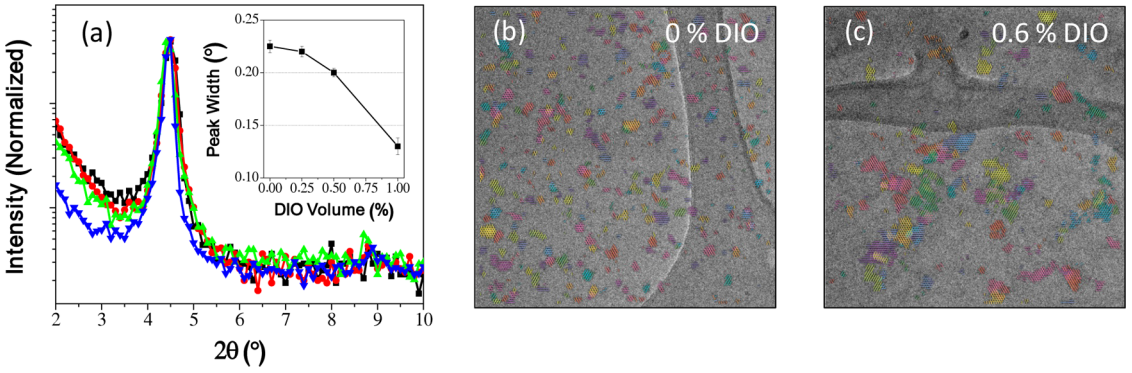


**Figure 6. (a) Out-of-plane X-ray diffraction of *p*-DTS(PTTh$_2$)$_2$:PC$_{71}$BM bulk heterojunction thin-films as a function of DIO concentration in the deposition solution. (Inset) Gaussian peak width of the $2\theta \sim 4.51°$ (d ~ 1.96 nm) scattering contribution. HR-TEM of the corresponding in-plane contributions for (b) 0% and (c) 0.6% DIO additive concentrations used during the deposition of *p*-DTS(PTTh$_2$)$_2$ thin-films. Colored lines have been added for clarity to denote the strength and directionality of the crystalline planes. A significant increase in the crystallite size is found for the 0% DIO sample compared to the 0.6% DIO sample. The side length of each TEM image is 656 nm.**

this factor, we conjecture that *p*-DTS(PTTh$_2$)$_2$ is preferentially textured in the vertical direction.

**A Comparison of PC$_{71}$BM, *p*-DTS(PTTh$_2$)$_2$ and *p*-DTS(PTTh$_2$)$_2$:PC$_{71}$BM Photoconductivity.** In neat materials, intrinsic processes are often considered to be masked by extrinsic effects on electron−hole pair dissociation. The purity of the PC$_{71}$BM used in this study was 99%, and yet clear evidence of the intermolecular or interband excitation was observed. In the case of *p*-DTS(PTTh$_2$)$_2$, the purity used in this study is estimated to be greater than 99.9% which suggests that photocarrier generation is likely not associated with impurities.[41] Furthermore, the photoconductive response in this system did not vary greatly with changes to [DIO] despite the significant changes to the crystallite sizes. This observation is consistent with ultrafast measurements, which indicate that within the DTS(PTTh$_2$)$_2$:PC$_{71}$BM BHJ materials, excitons diffuse over distances of 10−20 nm at time scales out to 1 ns, while pure *p*-DTS(PTTh$_2$)$_2$ materials only show polaron formation at time scales of <1 ps.[22] Collectively, these observations signify that the photoconductive properties of *p*-DTS(PTTh$_2$)$_2$ observed in this study are intrinsic in nature and thus do not rely on exciton diffusion to impurities, interfaces, or defects as a prerequisite to free carrier formation following absorption.

The absorption spectrum in such molecules originates from an intramolecular transition from the highest occupied molecular orbital (HOMO) to the lowest unoccupied molecular orbital (LUMO). Within molecular solids, strong intermolecular electronic coupling is required to delocalize the carriers sufficiently to enable significant photoconductivity at room temperature.[42] The observed high intrinsic photoresponse and the nearly quantitative spectral agreement between the photoconductive response and absorptance suggest this to be true for *p*-DTS(PTTh$_2$)$_2$ thin-films.

The archetypal molecular system, pentacene, also exhibits wavelength-independent quantum efficiencies for carrier generation[43] and ultrafast photocarrier generation.[44] Both of these observations are consistent with strong-intermolecular interactions as evidenced by experimental and theoretical studies which have indicated[45] and predicted,[24] respectively, that the exciton binding energies are as low as ~0.1 eV. On the basis of the above findings, a comparable exciton binding energy would be expected for DTS(PTTh$_2$)$_2$.

The similarity between pentacene and *p*-DTS(PTTh$_2$)$_2$ suggests a common mechanism to the photocarriers formation in these systems. Recent ultrafast (0.01−100 ps) measurements of the polarization anisotropy of the photoinduced absorption have provided evidence that the major optical properties of *p*-DTS(PTTh$_2$)$_2$ result from the photoexcitation of a single molecule, but that the photoexcitation process enables electron and hole delocalization along the $\pi$-stacking direction within the crystal structure.[22] Thus, the photoexcitation mechanism in *p*-DTS(PTTh$_2$)$_2$ is characteristic of Frenkel exciton theory with strong intermolecular coupling due to $\pi$-stacking in the solid-state.

Within this theory, the extent of intrinsic carrier generation is determined by the branching ratio between delocalization, governed through the intermolecular coupling, and localization, dictated by exciton−phonon coupling and disorder.[42,46,47] When incorporated into donor−acceptor BHJ materials, the intrinsic nature of the carrier formation process within such small-molecule systems is overwhelmed by the highly efficient interfacial charge-transfer (CT) processes.[1,2] The high sensitivity of these latter processes to the nanostructured morphology in such BHJs is demonstrated by the significant variation of the *p*-DTS(PTTh$_2$)$_2$:PC$_{71}$BM photoconductive response upon slight changes to the [DIO]. A comparison of the quantum efficiencies for photocarrier collection highlights that, at the optimum 0.25% DIO v/v, the sensitization effect of the PC$_{71}$BM on the *p*-DTS(PTTh$_2$)$_2$ in the BHJ yields a $10^3$ and $10^2$ fold enhancement to their photoconductive response compared to the neat films, respectively (see Supporting Information, Figure S4).

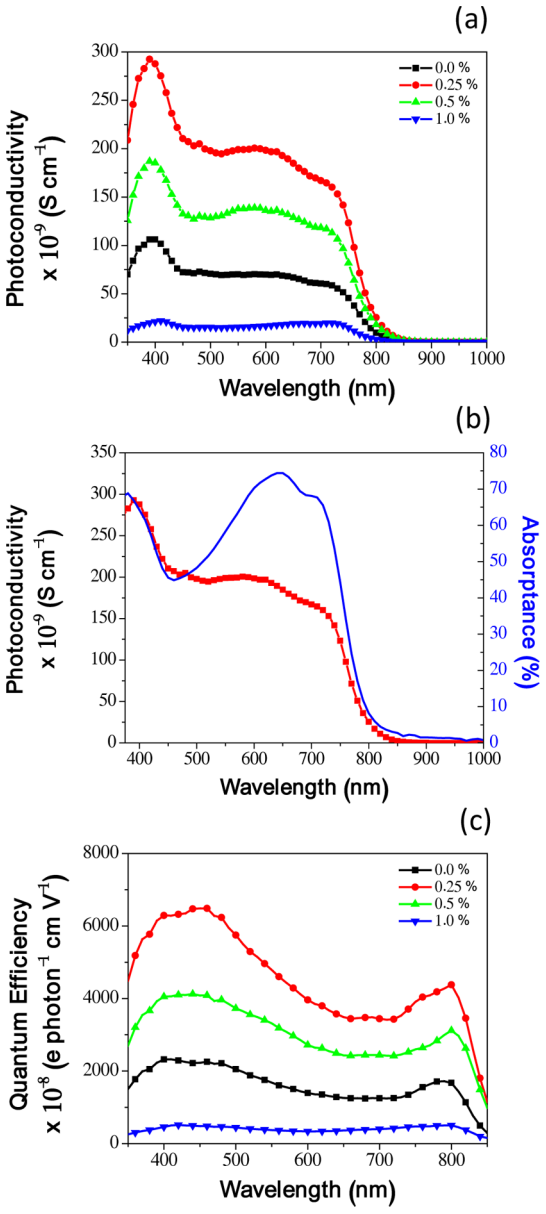


**Figure 7. (a) Steady-state photoconductive profiles of *p*-DTS(PTTh$_2$)$_2$:PC$_{71}$BM as a function of DIO concentration. The photocurrents were renormalized to a constant incident photon flux of $10^{14}$ photons/cm$^2$ s (b) A comparison of the photoconductive response (red squares) of *p*-DTS(PTTh$_2$)$_2$:PC$_{71}$BM with 0.25% DIO and its absorptance spectrum (—). (c) Calculated electric field dependent quantum yields for photocarrier collection for *p*-DTS(PTTh$_2$)$_2$:PC$_{71}$BM as a function of DIO concentration in the system. These yields were validated for electric fields up to $2 \times 10^4$ V/cm.**

This enhancement of the photoconductivity must arise from either variation to the mobility or the density of collected carriers (see eq 1). Field effect measurements were conducted to evaluate the carrier mobilities within the investigated systems (see Supporting Information, Table S1). These measurements yielded hole mobilities of neat *p*-DTS(PTTh$_2$)$_2$ and that blended with PC$_{71}$1BM, both at 0.25% v/v DIO, of $\sim 3 \times 10^{-2}$ cm$^2$/(V s) and $\sim 2 \times 10^{-3}$ cm$^2$/(V s), respectively. Meanwhile, analogous measurements of electron mobility provided reliable values only for PC$_{71}$BM, $6 \times 10^{-4}$ cm$^2$/(V s), and its blend with *p*-DTS(PTTh$_2$)$_2$, $7 \times 10^{-4}$ cm$^2$/(V s). The lowering of the hole mobility and the increase of the electron mobility due to the fullerene component in the BHJs as compared to neat *p*-DTS(PTTh$_2$)$_2$, indicates that the major cause of the photoconductive enhancement results from an increase in the density of collected carriers. By considering that the FET derived mobilities provide an upper limit to their true time-averaged values within the thin-films, we calculate that the enhancement to the density of collected carriers in the optimum BHJ composition compared to the neat *p*-DTS(PTTh$_2$)$_2$ system is $\sim 10^3$.

The relative level of sensitization in these systems is comparable to that of fullerenes on conjugated polymers such as *rr*-P3HT or PCPDTBT (poly[2,6-(4,4-bis-(2-ethylhexyl)-4*H*-cyclopenta[2,1-*b*;3,4-*b*']dithiophene)-*alt*-4,7-(2,1,3-benzothiadiazole)]).[48] However, one of the striking features of this small-molecule system is that the absolute quantum efficiency for photo carrier collection at an equivalent electric field is approximately 1 order of magnitude higher for the neat *p*-DTS(PTTh$_2$)$_2$ and its blends with PC$_{71}$BM than for the above polymer donor systems. As the charge carrier mobilities are similar in these materials, this enhancement must originate from differences in recombination lifetimes and/or internal carrier generation yields.[32] To elucidate between these two factors, time-resolved photoconductivity studies are necessary and will be the basis of future work.

## CONCLUSIONS

By combining studies of the morphology, photoconductivity, and charge transport properties of PC$_{71}$BM, *p*-DTS(PTTh$_2$)$_2$ and *p*-DTS(PTTh$_2$)$_2$:PC$_{71}$BM bulk heterojunctions as a function of the additive diiodoctane, we have been able to gain insight into the photoexcitation and transport mechanisms in such systems. In the case of PC$_{71}$BM, the limited structural variation provided by the additive did not greatly influence the photoconductive response. Despite this, we were able to approximate the exciton binding energy in this system to be $\sim$0.45 eV, a value that is comparable to that determined from photoelectron spectroscopy.

For neat *p*-DTS(PTTh$_2$)$_2$, diiodooctane had a strong impact on the evolution of the morphology, but still resulted in a limited influence on the photoconductive response. This was attributed to the intrinsic nature of charge generation in these materials and the limited variation to carrier mobility across this additive range. When these results were considered in conjunction with available ultrafast spectroscopic data, we concluded that the absorption in the visible region of the spectrum event in *p*-DTS(PTTh$_2$)$_2$ is characteristic of a Frenkel exciton, with significant delocalization of the

electronic structure due to electronic intermolecular interactions along the $\pi-\pi$ stacking direction. The high magnitude of the photoconductivity at room temperature and its spectral characteristics imply that the Coulomb binding energy between electrons and holes along the $\pi-\pi$ stacking direction in *p*-DTS-$(PTTh_2)_2$ is not more than a few $k_BT$.

Finally, the photoconductive responses of the small-molecule bulk heterojunctions were found to be highly sensitive to the additive concentration due to its affect on the nanoscale morphology. Under optimized morphologies, enhancements to the photoconductive responses of up to $10^3$ were found with respect to their neat films. While such enhancements are comparable to traditionally studied $\pi$-conjugated polymers that are sensitized by fullerenes, the nearly 10-fold increase in the quantum efficiencies at comparable electric fields within these small-molecule systems makes them more promising candidates for use within next-generation photoconductivity-based applications.

## METHODS

**Thin Film Preparation.** Thin-films of *p*-DTS$(PTTh_2)_2$, $PC_{71}BM$ (99%, Solenne), and 7:3 *p*-DTS$(PTTh_2)_2$:$PC_{71}BM$ (w/w) were deposited onto precleaned, UV-ozone treated low-sodium glass substrates *via* spin-coating from 40 mg/mL solutions in chlorobenzene (99%, Sigma-Aldrich, anhydrous) with concentration of DIO (98%, Sigma-Aldrich) vaying between 0 and 1% (v/v). As deposited films (~150−180 nm) were dried at 70 °C for 10 min prior to being loaded into a Angstrom thermal evaporator. Au strip electrodes with channel dimensions of 750 $\mu$m (width) × 75 $\mu$m (length) were deposited through a shadow mask at a base pressure of $4 \times 10^{-6}$ Torr. All sample preparation steps were carried out under inert conditions (<10 ppm $O_2$, <0.1 ppm $H_2O$).

**Photoconductivity Measurements.** For photoconductivity measurements, samples were loaded into a home-built vacuum chamber directly attached to a turbo pump. A brief exposure to air (<1 min) was necessary to load the samples. A monochromated tungsten lamp, which was mechanically chopped (Stanford Research Instruments SR540 chopper) at 138 Hz, was incident on the sample. The incident light intensity was in the 10−50 $\mu W/cm^2$ range. Photocurrent was detected through a lock-in amplifier (Stanford Research Instruments SR830), with the sample biased externally using a Keithly voltmeter. The photocurrent responses of all samples were measured with illumination through the glass and within the linear photoresponse range. The incident light power was measured using a calibrated Si *p-i-n* photodiode. On the basis of this, the experimental photocurrents were renormalized for a constant photon flux of $10^{14}$ photon/($cm^2$ s). This value was approximately equal to that illuminating the samples across the wavelength range studied.

**Field-Effect Measurements.** Heavily doped silicon substrates with 200 nm $SiO_2$ were used as a bottom gate electrode and insulating dielectric. A passivation layer of poly(propalene-*co*-1-butane) (PPCB, about 4% in anhydrous decahydronaphthalene) was spun on top of $SiO_2$ at 6000 rpm. Neat *p*-DTS$(PTTh_2)_2$ and blends of p-DTS$(PTTh_2)_2$:$PC_{71}BM$ (7:3 w/w) at an 8 mg/mL concentration in chlorobenzene were prepared with a volume fraction of 0%, 0.25%, 0.5%, and 1% diiodooctane (DIO). Blended solutions were heated at 80 °C for 2 h, cooled to room-temperature, spin-coated onto PPCB passivated substrates at 2000 rpm and finally baked at 70 °C for 10 min. Thermally evaporated silver contacts were then deposited through a shadow mask onto the BHJ active layer. All the FET test was done in a nitrogen environment, $O_2$ level < 2 ppm, and was measured by Keithley 4200 system. Electron mobilities for the above systems and $PC_{71}BM$ (also deposited from an 8 mg/mL chlorobenzene solution) were carried out with comparable preparations except that aluminum was used as the thermally evaporated metal contact.

**Thin-Film Characterization.** Out-of-plane X-ray diffraction measurements were carried out on a Rigaku Smartlab High-Resolution Diffractometer with a Cu K α source (wavelength of 1.5405 Å) using $2\theta$ step of 0.1°. These were made on the same samples as the photoconductivity measurements. The absorptance of each film was determined directly from the known transmittance and reflectance which were obtained using a Perkin-Elmer Lambda 780 NIR-UV−vis spectrometer coupled to an integrating sphere attachment.

**Transmission Electron Microscopy.** The donor thin films were cast from 20 mg/mL with the appropriate DIO v/v ratio onto PEDOT:PSS coated silicon wafers to give thicknesses of ~100 nm. The films were baked at 70 °C for 10 min than allowed to stand for more than a day. The films were slowly submerged into DI water and delaminated onto the air−water interface. These were then broken into smaller pieces and transferred to a C-Flat TEM grid with an array of 2 $\mu$m holes. To aid focusing of the electron beam, the TEM grids were soaked in a solution of 15 nm citrate stabilized gold nanoparticles and washed with isopropyl alcohol prior to film transfer. The preparation and imaging of the BHJ thin films is detailed elsewhere.[11] HR-TEM images were acquired near the optimal underfocus condition for the ~2 nm peak of the donor. All HR-TEM experiments were performed on an FEI Titan operating at 300 kV.

*Conflict of Interest:* The authors declare no competing financial interest.

*Acknowledgment.* This research was carried out at UCSB with support from the Department of Energy under a grant titled "Charge Recombination, Transport Dynamics, and Interfacial Effects in Organic Solar Cells"; DOE #DE-FG02-08ER46535. The design and synthesis of *p*-DTS$(PTTh_2)_2$ was carried out by Prof. G. Bazan and Dr. Greg Welch with support from the Center for Energy Efficient Materials, an Energy Frontier Research Center funded by the Office of Basic Energy Sciences of the US Department of Energy (DE-DC0001009). The TEM studies were supported by the National Science Foundation (DMR-0856060). The authors would like to acknowledge Dr. L. Kaake and Dr. Y. Sun for useful discussions during the preparation of this manuscript. J.J. wishes to acknowledge financial support through CSIRO, Australian Research Council for support through the APD Grant DP110105341, the Australian Solar Institute USASEC research exchange program, and the Fulbright Postdoctoral Fellowship.

*Supporting Information Available:* Transmittance, reflectance and absorptance of neat and blended films, photoconductive response of $PC_{71}BM$ in the presence of the quenching gas $CO_2 + SF_6$ (9:1), selected area electron diffraction of *p*-DTS$(PTTh_2)_2$, photoconductivity and absorptance spectral profile matching of *p*-DTS$(PTTh_2)_2$, cyclic voltammetry of *p*-DTS$(PTTh_2)_2$, comparison of neat and blend photoconductive responses, and field-effect transistor charge mobilities. This material is available free of charge *via* the Internet at http://pubs.acs.org.

## REFERENCES AND NOTES

1. Yu, G.; Gao, J.; Hummelen, J. C.; Wudl, F.; Heeger, A. J. Polymer Photovoltaic Cells: Enhanced Efficiencies *via* a Network of Internal Donor−Acceptor Heterojunctions. *Science* **1995**, *270*, 1789–1791.
2. Halls, J. J. M.; Walsh, C. A.; Greenham, N. C.; Marseglia, E. A.; Friend, R. H.; Moratti, S. C.; Holmes, A. B. Efficient Photodiodes from Interpenetrating Polymer Networks. *Nature* **1995**, *376*, 498–500.

3. Shaheen, S. E.; Brabec, C. J.; Sariciftci, N. S.; Padinger, F.; Fromherz, T.; Hummelen, J. C. 2.5% Efficient Organic Plastic Solar Cells. *Appl. Phys. Lett.* **2001**, *78*, 841–843.
4. Ma, W.; Yang, C.; Gong, X.; Lee, K.; Heeger, A. J. Thermally Stable, Efficient Polymer Solar Cells with Nanoscale Control of the Interpenetrating Network Morphology. *Adv. Funct. Mater.* **2005**, *15*, 1617–1622.
5. Li, G.; Shrotriya, V.; Huang, J.; Yao, Y.; Moriarty, T.; Emery, K.; Yang, Y. High-Efficiency Solution Processable Polymer Photovoltaic Cells by Self-Organization of Polymer Blends. *Nat. Mater.* **2005**, *4*, 864–868.
6. Peet, J.; Kim, J. Y.; Coates, N. E.; Ma, W. L.; Moses, D.; Heeger, A. J.; Bazan, G. C. Efficiency Enhancement in Low-Bandgap Polymer Solar Cells by Processing with Alkane Dithiols. *Nat. Mater.* **2007**, *6*, 497–500.
7. Lee, J. K.; Ma, W. L.; Brabec, C. J.; Yuen, J.; Moon, J. S.; Kim, J. Y.; Lee, K.; Bazan, G. C.; Heeger, A. J. Processing Additives for Improved Efficiency from Bulk Heterojunction Solar Cells. *J. Am. Chem. Soc.* **2008**, *130*, 3619–3623.
8. Lou, S. J.; Szarko, J. M.; Xu, T.; Yu, L.; Marks, T. J.; Chen, L. X. Effects of Additives on the Morphology of Solution Phase Aggregates Formed by Active Layer Components of High-Efficiency Organic Solar Cells. *J. Am. Chem. Soc.* **2011**, *133*, 20661–20663.
9. Rogers, J. T.; Schmidt, K.; Toney, M. F.; Bazan, G. C.; Kramer, E. J. Time-Resolved Structural Evolution of Additive-Processed Bulk Heterojunction Solar Cells. *J. Am. Chem. Soc.* **2012**, *134*, 2884–2887.
10. Agostinelli, T.; Ferenczi, T. A. M.; Pires, E.; Foster, S.; Maurano, A.; Müller, C.; Ballantyne, A.; Hampton, M.; Lilliu, S.; Campoy-Quiles, M.; *et al*. The Role of Alkane Dithiols in Controlling Polymer Crystallization in Small Band Gap Polymer:Fullerene Solar Cells. *J. Polym. Sci., Part B: Polym. Phys.* **2011**, *49*, 717–724.
11. Sun, Y.; Welch, G. C.; Leong, W. L.; Takacs, C. J.; Bazan, G. C.; Heeger, A. J. Solution-Processed Small-Molecule Solar Cells with 6.7% Efficiency. *Nat. Mater.* **2012**, *11*, 44–48.
12. Clarke, T. M.; Durrant, J. R. Charge Photogeneration in Organic Solar Cells. *Chem. Rev.* **2010**, *110*, 6736–6767.
13. Sariciftci, N. S.; Smilowitz, L.; Heeger, A. J.; Wudl, F. Photoinduced Electron Transfer from a Conducting Polymer to Buckminsterfullerene. *Science* **1992**, *258*, 1474–1476.
14. Banerji, N.; Cowan, S.; Leclerc, M.; Vauthey, E.; Heeger, A. J. Exciton Formation, Relaxation, and Decay in PCDTBT. *J. Am. Chem. Soc.* **2010**, *132*, 17459–17470.
15. Sinclair, M.; Moses, D.; Heeger, A. J. Picosecond Photoconductivity in *trans*-Polyacetylene. *Solid State Commun.* **1986**, *59*, 343–347.
16. Lee, C. H.; Yu, G.; Moses, D.; Heeger, A. J. Picosecond Transient Photoconductivity in Poly(*p*-phenylenevinylene). *Phys. Rev. B: Condens. Matter* **1994**, *49*, 2396–2407.
17. Moses, D.; Sinclair, M.; Heeger, A. J. Carrier Photogeneration and Mobility in Polydiacetylene: Fast Transient Photoconductivity. *Phys. Rev. Lett.* **1987**, *58*, 2710–2713.
18. Moses, D.; Okumoto, H.; Lee, C. H.; Heeger, A. J.; Ohnishi, T.; Noguchi, T. Mechanism of Carrier Generation in Poly(phenylene vinylene): Transient Photoconductivity and Photoluminescence at High Electric Fields. *Phys. Rev. B* **1996**, *54*, 4748–4754.
19. Österbacka, R.; An, C. P.; Jiang, X. M.; Vardeny, Z. V. Two-Dimensional Electronic Excitations in Self-Assembled Conjugated Polymer Nanocrystals. *Science* **2000**, *287*, 839–842.
20. Bakulin, A. A.; Rao, A.; Pavelyev, V. G.; van Loosdrecht, P. H. M.; Pshenichnikov, M. S.; Niedzialek, D.; Cornil, J.; Beljonne, D.; Friend, R. H. The Role of Driving Energy and Delocalized States for Charge Separation in Organic Semiconductors. *Science* **2012**, *335*, 1340–1344.
21. Ostroverkhova, O.; Cooke, D. G.; Shcherbyna, S.; Egerton, R. F.; Hegmann, F. A.; Tykwinski, R. R.; Anthony, J. E. Band-like Transport in Pentacene and Functionalized Pentacene Thin Films Revealed by Subpicosecond Transient Photoconductivity Measurements. *Phys. Rev. B: Condens. Matter* **2005**, *71*, 035204.
22. Kaake, L. G.; Jasieniak, J. J.; Bakus II, R. C.; Moses, D.; Welch, G. C.; Bazan, G. C.; Heeger, A. J., submitted **for publication 2012**.
23. Kirova, N.; Brazovskii, S.; Bishop, A. R. A Systematic Theory for Optical Properties of Phenylene-Based Polymers. *Synth. Met.* **1999**, *100*, 29–53.
24. Hummer, K.; Ambrosch-Draxl, C.; Bussi, G.; Ruini, A.; Caldas, M. J.; Molinari, E.; Laskowski, R.; Christensen, N. E. *Ab-Initio* Study of Excitonic Effects in Conventional and Organic Semiconductors. *Phys. Status Solidi B* **2005**, *242*, 1754–1758.
25. Arkhipov, V. I.; Bässler, H. Exciton Dissociation and Charge Photogeneration in Pristine and Doped Conjugated Polymers. *Phys. Status Solidi A* **2004**, *201*, 1152–1187.
26. Moses, D.; Schmechel, R.; Heeger, A. J. Effects of Structural Disorder and Temperature on the Distribution of Exciton Binding Energy in Poly(phenylene vinylene) Films. *Synth. Met.* **2003**, *139*, 807–810.
27. Korovyanko, O. J.; Österbacka, R.; Jiang, X. M.; Vardeny, Z. V.; Janssen, R. A. J. Photoexcitation Dnamics in Regioregular and Regiorandom Polythiophene Films. *Phys. Rev. B: Condens. Matter* **2001**, *64*, 235122.
28. Pakbaz, K.; Lee, C. H.; Heeger, A. J.; Hagler, T. W.; McBranch, D. Nature of the Primary Photoexcitations in Poly(arylene-vinylenes). *Synth. Met.* **1994**, *64*, 295–306.
29. Beaujuge, P. M.; Fréchet, J. M. J. Molecular Design and Ordering Effects in $\pi$-Functional Materials for Transistor and Solar Cell Applications. *J. Am. Chem. Soc.* **2011**, *133*, 20009–20029.
30. Welch, G. C.; Perez, L. A.; Hoven, C. V.; Zhang, Y.; Dang, X.-D.; Sharenko, A.; Toney, M. F.; Kramer, E. J.; Nguyen, T.-Q.; Bazan, G. C. A Modular Molecular Framework for Utility in Small-Molecule Solution-Processed Organic Photovoltaic Devices. *J. Mater. Chem.* **2011**, *21*, 12700–12709.
31. Kaake, L. G.; Welch, G. C.; Moses, D.; Bazan, G. C.; Heeger, A. J. Influence of Processing Additives on Charge-Transfer Time Scales and Sound Velocity in Organic Bulk Heterojunction Films. *J. Phys. Chem. Lett.* **2012**, 1253–1257.
32. Bube, R. H., *Photoconductivity of Solids*, 1st ed.; John Wiley & Sons: NJ, 1960.
33. Moses, D. Transient Photoconductivity of a-Se Measured by the Time-of-Flight and Stripline-Switch Techniques: A Comparative Study. *Philos. Mag. B* **1992**, *66*, 1–14.
34. Verploegen, E.; Mondal, R.; Bettinger, C. J.; Sok, S.; Toney, M. F.; Bao, Z. Effects of Thermal Annealing Upon the Morphology of Polymer−Fullerene Blends. *Adv. Funct. Mater.* **2010**, *20*, 3519–3529.
35. Moses, D.; Soci, C.; Miranda, P.; Heeger, A. J. The Role of Electron Photoemission in the 'Photoconductivity' of Semiconducting Polymers. *Chem. Phys. Lett.* **2001**, *350*, 531–536.
36. Lof, R. W.; van Veenendaal, M. A.; Koopmans, B.; Jonkman, H. T.; Sawatzky, G. A. Band Gap, Excitons, and Coulomb Interaction in Solid $C_{60}$. *Phys. Rev. Lett.* **1992**, *68*, 3924–3927.
37. Ratcliff, E. L.; Meyer, J.; Steirer, K. X.; Armstrong, N. R.; Olson, D.; Kahn, A. Energy Level Alignment in PCDTBT:PC70BM Solar Cells: Solution Processed NiO*x* for Improved Hole Collection and Efficiency. *Org. Electron.* **2012**, *13*, 744–749.
38. Collins, B. A.; Cochran, J. E.; Yan, H.; Gann, E.; Hub, C.; Fink, R.; Wang, C.; Schuettfort, T.; McNeill, C. R.; Chabinyc, M. L.; *et al*. Polarized X-ray Scattering Reveals Non-crystalline Orientational Ordering in Organic Films. *Nat. Mater.* **2012**, *11*, 536–543.
39. Zhang, X.; Richter, L. J.; DeLongchamp, D. M.; Kline, R. J.; Hammond, M. R.; McCulloch, I.; Heeney, M.; Ashraf, R. S.; Smith, J. N.; Anthopoulos, T. D.; *et al*. Molecular Packing of High-Mobility Diketo Pyrrolo−Pyrrole Polymer Semiconductors with Branched Alkyl Side Chains. *J. Am. Chem. Soc.* **2011**, *133*, 15073–15084.
40. Preliminary results suggest that long-range order is observed for the in-plane pi−pi population. This suggests that some structural similarities to the neat films persist within the blends; a discussion of which will be the subject of future work.
41. Leong, W. L.; Welch, G. C.; Kaake, L. G.; Takacs, C. J.; Sun, Y.; Bazan, G. C.; Heeger, A. J. Role of Trace Impurities in the Photovoltaic Performance of Solution Processed Small-Molecule Bulk Heterojunction Solar Cells. *Chem. Sci.* **2012**, *3*, 2103–2109.

42. Scholes, G. D. Insights into Excitons Confined to Nanoscale Systems: Electron−Hole Interaction, Binding Energy, and Photodissociation. *ACS Nano* **2008**, *2*, 523–537.
43. Gao, J.; Hegmann, F. A. Bulk Photoconductive Gain in Pentacene Thin Films. *Appl. Phys. Lett.* **2008**, *93*, 223306.
44. Ostroverkhova, O.; Cooke, D. G.; Hegmann, F. A.; Anthony, J. E.; Podzorov, V.; Gershenson, M. E.; Jurchescu, O. D.; Palstra, T. T. M. Ultrafast Carrier Dynamics in Pentacene, Functionalized Pentacene, Tetracene, and Rubrene Single Crystals. *Appl. Phys. Lett.* **2006**, *88*, 162101.
45. Kaur, I.; Jia, W.; Kopreski, R. P.; Selvarasah, S.; Dokmeci, M. R.; Pramanik, C.; McGruer, N. E.; Miller, G. P. Substituent Effects in Pentacenes: Gaining Control over HOMO−LUMO Gaps and Photooxidative Resistances. *J. Am. Chem. Soc.* **2008**, *130*, 16274–16286.
46. Fidder, H.; Knoester, J.; Wiersma, D. A. Optical Properties of Disordered Molecular Aggregates: A Numerical Study. *J. Chem. Phys.* **1991**, *95*, 7880–7890.
47. Scholes, G. D.; Rumbles, G. Excitons in Nanoscale Systems. *Nat. Mater.* **2006**, *5*, 683–696.
48. Soci, C.; Hwang, I. W.; Moses, D.; Zhu, Z.; Waller, D.; Gaudiana, R.; Brabec, C. J.; Heeger, A. J. Photoconductivity of a Low-Bandgap Conjugated Polymer. *Adv. Funct. Mater.* **2007**, *17*, 632–636.